Predicting novel atomic structure of the lowest-energy Fe_nP_{13-n} ($n = 0$–13) clusters: A new parameter for characterizing chemical stability

Yuanqi Jiang(蒋元祺)[1,†] and Ping Peng(彭平)[2]

[1] *College of Physics & Electronic Information, Nanchang Normal University, Nanchang* 330032, *China*
[2] *School of Material Science & Engineering, Hunan University, Changsha* 410082, *China*

(Received 5 November 2022; revised manuscript received 18 December 2022; accepted manuscript online 27 December 2022)

A series of novel atomic structure of lowest-energy Fe_nP_{13-n} ($n = 0$–13) clusters via density functional theory (DFT) calculations and an unbiased structure search using Crystal structure AnaLYsis by Particle Swarm Optimization (CALYPSO) code. Our research results show that the global minimum geometry structure of neutral $Fe_{13-n}P_n$ ($n = 0$–6) clusters tend to form cage structures but the lowest-energy $Fe_{13-n}P_n$ ($n = 7$–13) clusters are gradually evolution from a cage structure to a chain shape geometric structure. Their geometric structure should responsible for the raise of binding energy from Fe_7P_6 to P_{13} clusters rather than chemical components. This is completely different from a linear relation of the binding energy with chemical components in our previous research for Cu_nZr_{13-n} ($n = 3$–10) clusters (*J. Mol. Liq.* **343** 117603 (2021)). Hence, in order to characterize the global chemical stability of target cluster, we proposed a new parameter (jyq $= \eta/\chi$) that the chemical hardness of isolated cluster is used to be divided by its electronegativity. One of the biggest advantages of this parameter is successful coupling the ability of a resistance to redistribution of electrons and the ability to attract electrons from other system (such as atom, molecular or metallic clusters). Moreover, it is found that the P_{13} cluster shows typical insulator characteristics but the $Fe_{12}P_1$ shows typical conductor characteristics, which phenomena can be attributed to the remarkable delocalized and localized electrons in $Fe_{12}P_1$ and P_{13}, respectively. In terms of nearly-free-electron mode, we also found that the number of electrons on Femi level ($N(E_F)$) are obviously tended to toward a lower value when Fe was replaced gradually with P from Fe_{13} to P_{13}, and a non-magnetic can be observed in Fe_{13}, Fe_2P_{11}, Fe_1P_{12}, and P_{13} that mainly because their perfect symmetrical between spin-up and spin-down of density of states of electrons.

Keywords: Fe–P cluster, density functional theory (DFT), ground-state structure, electronic structure

PACS: 71.15.Mb, 36.40.Mr, 36.40.−c, 31.15.ae **DOI:** 10.1088/1674-1056/acae75

1. Introduction

At present, the heat of study on the ground state geometry structure and electronic structure of isolated metal clusters start to descend year by year,[1–3] which mainly due to below three reasons. First, there is absence of important scientific problems that need to be urgently solved in the field of cluster science, which is a crucial for the cluster science whether can continue to move forward in the future.[4] Second, after years of research, although there are abundant research results on the ground state geometry and electronic structure of small and medium-sized free metal clusters,[1,2] there are few systematic review articles.[1,2,4] It is well known that a timely summary and reflection are crucial to the development of the field. Third, compared with many years ago, although the computing power of the computer has been greatly improved, the research of the geometry and electronic structure of metallic clusters with larger-scale is still time-consuming and challenging by first principles calculations.

Metallic glasses (MGs) have drawn considerable attention as promising structural materials due to their unique combination of properties such as high strength and extreme hardness.[5,6] However, the limited ductility of MGs restricts their use in various structural and engineering field.[5] Lots of scientists have been made to unravel the physics of deformation and fracture for these MGs. Notably the Fe–P MGs appears to be one of the few models of an amorphous alloy that results in brittle behavior on the atomic scale, making it an attractive binary system for examining a range of mechanical response regimes using atomic simulations. Even so, controversies remain about the failure and fracture mechanisms of Fe–P MGs from the perspective of atomic clusters up to now. Such as how do the atomic cluster to influence the fracture behavior of MGs during the tension and compression?

Based on the background mentioned above, by combining crystal structure analysis by particle swarm optimization (CALYPSO)[7–9] code and DFT calculations,[10–12] we had carried out a series of studies on the ground state geometry and electronic structure of small and medium-sized free clusters, which often play a key role in the processes of rapid solidification of liquids metal. In this study, by CALYPSO searches[7–9,13] and DFT calculations, we also provide an extensive and systematic theoretical study on a series of

†Corresponding author. E-mail: yuanqi325@163.com
© 2023 Chinese Physical Society and IOP Publishing Ltd

Fe_nP_{13-n} ($n = 0$–13) clusters in order to examine how do the chemical components *versus* geometric structure to influence the energy stability as well as chemical stability of metallic glass.[14,15] And a special attention will be paid on the electronic structure and chemical activity in those lowest energy atomic clusters.[16] We believe that the study will help to gain a fundamental understanding of the unique phenomena in Fe–P metallic glass at the atomic and electronic scale. The study is organized as follows: in Section 2, we briefly mention computational details used. In Section 3 we discuss our results, and summarize the results in Section 4.

2. Computational methods

It is well known that determining the global minimum energy configuration of cluster is a notoriously challenged work, in this study, the lowest-energy structure of medium size of neutral Fe_nP_{13-n} ($n = 0$–13) clusters was searched in terms of CALYPSO[7–9] code. In particular, the entire ground-state geometric configuration search via CALYPSO code for hunting Fe_nP_{13-n} ($n = 0$–13) clusters mainly comprised three steps. First, the original configuration of Fe–P cluster was randomly generated with the restraint of point group symmetries, then the bond characterization matrix[7–9] was applied to examine the similarity of the generated configuration. After the first cluster population was generated, local structural optimizations were performed immediately by DFT calculations to eliminate the higher-energy landscape and accelerate the systems into a local minimum for conveniently generating the next population. Next, several low-energy structures, approximately 60% of the population size on the most promising areas of the search space, were retained to generate new structures by particle swarm optimization (PSO). Approximately 40% were randomly generated[17] using the symmetric constraints to maintain the diversity of the Fe–P clusters. In the processes of the structure search for each given Fe–P cluster, we followed approximately 45 generations of the structure prediction and obtained approximately 1350 isomers of Fe–P clusters, all of which were preliminary optimized and ordered in terms of the enthalpy by DFT calculations at 0 K. Accordingly, we had calculated and optimized more than 18900 cluster isomers from Fe_{13} to P_{13}. Eventually, DMOL^3 soft[18,19] was applied to optimize the top 5 lower-energy structures for each given Fe–P cluster in order to find the lowest-energy configuration. During DFT optimization and total energy calculation, electronic exchange–correlation functions represented in reciprocal space with the Perdew–Burke–Ernzerhof (PBE)[20,21] functional based on the generalized gradient approximation (GGA)[20,21] was used. A double-numerical basis set together with *d*-polarization functions (DNP) was selected to describe the electronic wave functions of Fe and P atoms. Only core electrons described by the DFT semi core pseudopots (DSPP) were calculated. All atomic positions in Fe–P clusters were relaxed by geometry optimization under a root-mean-square (RMS) force of 0.002 Ha/Å (1 Ha = 27.2114 eV) and RMS displacement of 0.005 Å. The calculations of the total energy and electronic structure were followed by the geometry optimization with a self-consistent field (SCF) tolerance of 1×10^{-5} Ha.

3. Results and discussion

3.1. Lowest-energy geometric structure of $Fe_{13-n}P_n$ ($n = 0$–13) clusters

We have combined the DFT calculations[14–16] and CALYPSO soft[7–9] to search the global minimum geometry structure of neutral $Fe_{13-n}P_n$ ($n = 0$–13) clusters. The lowest-energy geometric structure of neutral $Fe_{13-n}P_n$ ($n = 0$–13) clusters in terms of chemical compositions with total binding energy and point group symmetry are plotted in Fig. 1. For $n = 0$, it can be seen in Fig. 1 that the Fe_{13} exhibits a standard icosahedron configuration with I_h symmetry, which is consistent with previous reported on the ground state geometry structure of isolated Fe_{13} cluster.[22] For $n = 1$, we notice that the ground state geometry structure of isolated $Fe_{12}P_1$ is distorted icosahedron configuration with C_5 symmetry, when the bottom Fe atom was replaced by P atom. For n =2, the ground state geometric structure of $Fe_{11}P_2$ cluster exhibits an irregular geometry configuration with C_1 symmetry including pentagonal bi-pyramid compose of Fe atoms. Moreover, with increasing of P atoms and decreasing of Fe atoms, an identical atomic packing pattern are exhibited in the geometric structures of Fe_1P_3, Fe_9P_4, and Fe_8P_5, which reveal that the change of just chemical components is not enough to affect the ground state geometries structure of $Fe_{10}P_3$, Fe_9P_4, and Fe_8P_5. When the number of Fe atoms are reduced to 7 and 6, respectively, Fe atoms are gradually beginning to occupy the central position of the Fe_7P_6–C_{3v} and Fe_6P_7–C_1, when those P atoms tend to be arranged at the periphery of Fe atoms. Meanwhile, for $n = 8$, we notice that the lowest-energy geometric structures of Fe_5P_8 has an identical geometric structure as Cu_6Zr_7 and Cu_8Zr_5[16] in our previous reported, which reveal that the corresponding geometry configuration has higher structure stability. Next, from the chemical composition for Fe_4P_9, all the geometric configurations of the Fe_3P_{10}, Fe_2P_{11}, Fe_1P_{12}, and P_{13} cluster are gradually changed from the previous nearly spherical structure (such as Fe_{13}) to the chain structure with decreasing of Fe atoms and the increasing of P atoms. There are plenty of reasons to believe that the unusual evolution of the ground state geometry of $Fe_{13-n}P_n$ ($n = 0$–13) cluster must imply some undiscovered physical laws and mechanisms up to now. We will study on the phenomenon in depth below.

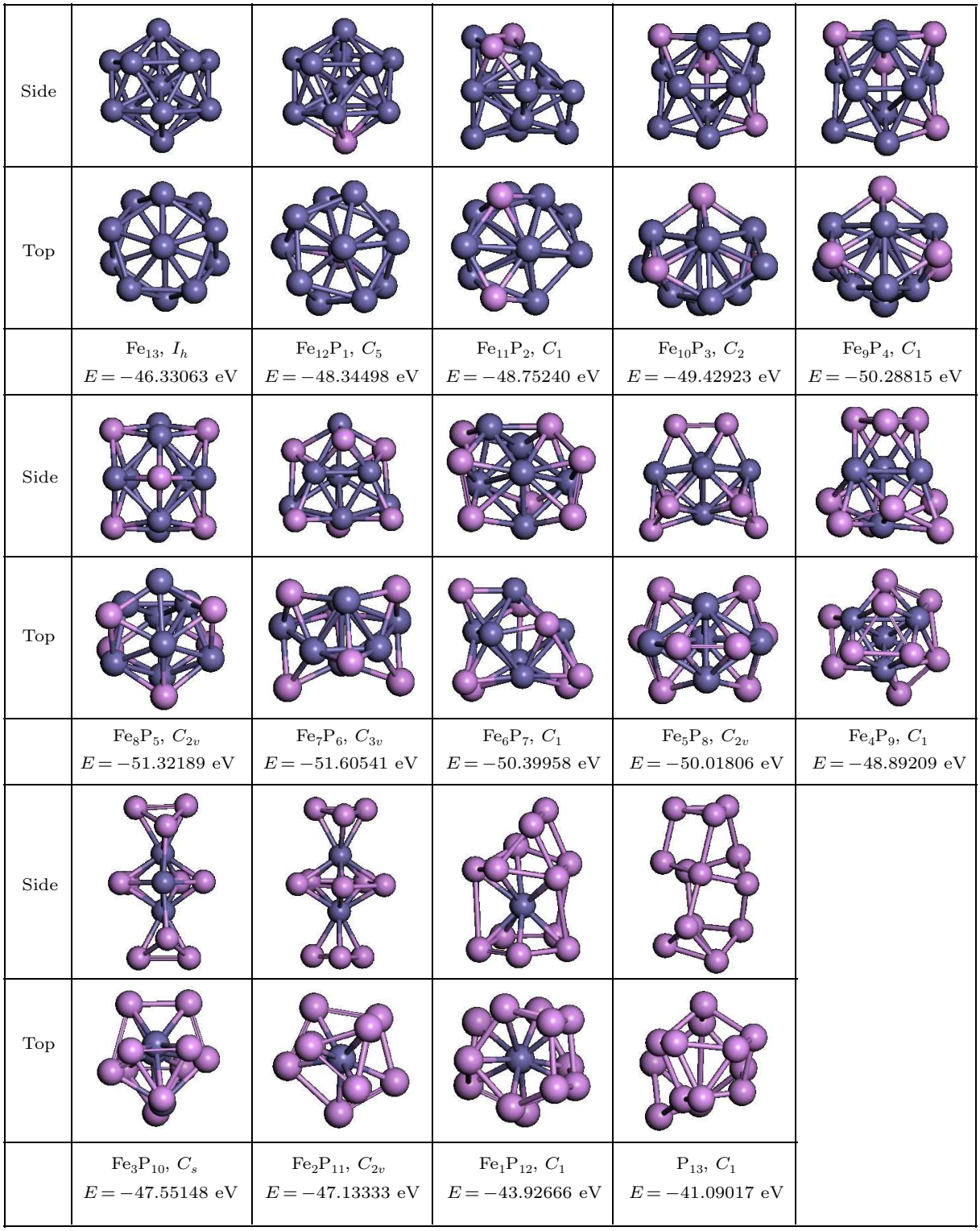


Fig. 1. The lowest-energy configuration of neutral $Fe_{13-n}P_n$ ($n = 0$–13) clusters in terms of chemical compositions with total binding energy and point group symmetry.

3.2. A new parameter for characterizing chemical stability of $Fe_{13-n}P_n$ ($n = 0$–13) clusters

From the perspective of thermodynamics, as definition, the total binding energies E_b of Fe–P clusters as a measure of the energy stability are firstly calculated by following equation:[16]

$$E_b = [E(Fe_{13-n}P_n) - nE(P) - (13-n)(Fe)], \quad (1)$$

where $E(Fe_{13-n}P_n)$ is the total energies of neutral $Fe_{13-n}P_n$ clusters, $E(Fe)$ and $E(P)$ are the energy of single gaseous Fe and P atoms, respectively. The size dependence of the E_b of the lowest-energy neutral, cation, and anion $Fe_{13-n}P_n$ ($n = 0$–13) clusters, respectively, are plotted in Fig. 2(a). From Fig. 2(a), one can see that the E_b of neutral, cation, and anion Fe–P clusters exhibits a consistent evolutionary rule. Namely,

their binding energy gradually reduce with decreasing of Fe and increasing of P from Fe_{13} to Fe_7P_6. Once the number of P atoms is greater than 6, the change of binding energy of Fe–P clusters shows the opposite trend, indicating the geometric configuration of Fe_7P_6 (C_{3v}) has the most energy advantage among all chemical components of $Fe_{13-n}P_n$ ($n = 0$–13) clusters. Which above phenomena indicate that the geometric structure should responsible for the raise of binding energy from Fe_7P_6 to P_{13} clusters rather than chemical components. This is completely different from a linear relation of the binding energy of Cu–Zr clusters with chemical components in Fig. 2(b).[16] Hence, in order to further investigate the competition and synergy between the chemical components and the geometric structure of Fe–P clusters, we further characterize the chemical stability based on the chemical hardness and chemical potential. In general, to facilitate the mathematical calculation for actual research, using the finite difference approximation,[16] the chemical potential and chemical hardness can be further express as follows:

$$\mu = -\frac{I+A}{2} = -\chi_{\mathrm{M}} = -\big[\big|E\left(\mathrm{Fe}_{13-n}\mathrm{P}_n\right) - E\left(\mathrm{Fe}_{13-n}\mathrm{P}_n\right)^{+}\big| + \big|E\left(\mathrm{Fe}_{13-n}\mathrm{P}_n\right) - E\left(\mathrm{Fe}_{13-n}\mathrm{P}_n\right)^{-}\big|\big]/2, \quad (2)$$

$$\eta = \frac{I-A}{2} = \big[\big|E\left(\mathrm{Fe}_{13-n}\mathrm{P}_n\right) - E\left(\mathrm{Fe}_{13-n}\mathrm{P}_n\right)^{+}\big| - \big|E\left(\mathrm{Fe}_{13-n}\mathrm{P}_n\right) - E\left(\mathrm{Fe}_{13-n}\mathrm{P}_n\right)^{-}\big|\big]/2. \quad (3)$$

Here $I = \big|E\left(\mathrm{Fe}_{13-n}\mathrm{P}_n\right) - E\left(\mathrm{Fe}_{13-n}\mathrm{P}_n\right)^{+}\big|$ and $A = \big|E\left(\mathrm{Fe}_{13-n}\mathrm{P}_n\right) - E\left(\mathrm{Fe}_{13-n}\mathrm{P}_n\right)^{-}\big|$ are the vertical ionization potential (VIP) and the vertical electron affinity (VEA) of neutral $Fe_{13-n}P_n$ clusters, respectively. $E\left(\mathrm{Fe}_{13-n}\mathrm{P}_n\right)^{+}$ and $E\left(\mathrm{Fe}_{13-n}\mathrm{P}_n\right)^{-}$ are the total energies of cationic and anionic $Fe_{13-n}P_n$ clusters, respectively, at the optimized geometry of the neutral cluster. On the one hand, in thermodynamics, chemical potential (μ) can be absorbed or released due to a change of the number of the atoms or electrons for given clusters, and the μ also can be used to predict the direction of chemical reaction, which can only happen from the side with higher μ to the side with lower μ until they are equal. Furthermore, if we put a minus sign in front of the μ in Eq. (2), it will naturally become Mulliken's electronegativity ($\chi_{\mathrm{M}} = (I+A)/2$). Meanwhile, because of this fundamental relation,[23–25] χ_{M} may can be called the absolute electronegativity.[23–25] As already mentioned, Pearson had proposed the χ_{M} can be applying to the whole system to attract electrons to itself, which may be an atom, a molecule, an ion, or a metal cluster.[23–25] On the other hand, the chemical stability of $Fe_{13-n}P_n$ clusters were also evaluated in terms of the chemical hardness η, which mathematical formula can be express as Eq. (3).[23–25]

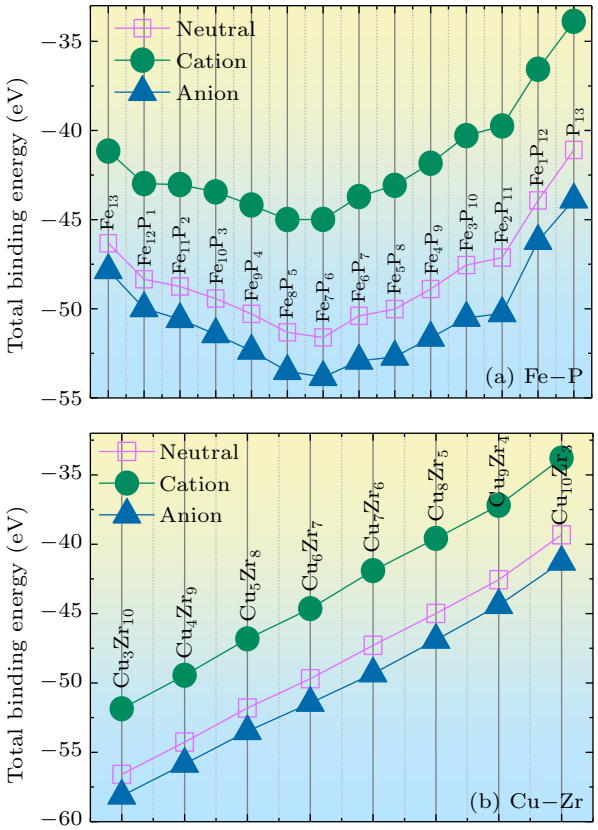


Fig. 2. Size dependence of the total binding energy E_{b} of the lowest-energy neutral, cation, and anion of (a) $Fe_{13-n}P_n$ ($n = 0$–13) clusters and (b) Cu_nZr_{13-n} ($n = 3$–10),[16] respectively.

Based on this, the electron count dependence of the calculated χ_{M} and η of the isolated $Fe_{13-n}P_n$ ($n = 0$–13) clusters are further plotted in Fig. 3, respectively. It is clearly shown that the η of $Fe_{13-n}P_n$ ($n = 0$–13) clusters exhibits a downward trend from P_{13} to Fe_{13} besides Fe_1P_{12} and Fe_7P_6 at the peak. Because η essentially represents a resistance to change in the electron distribution in metal clusters,[16,23] the chemical hardness of Fe_1P_{12} and Fe_7P_6 show a local maximum peak, respectively, which indicate they have relatively higher chemical stability in terms of the principle of maximum hardness,[20–23] *i.e.*, the even number of valence electron of Fe_1P_{12} (68) and Fe_7P_6 (86) should be responsible for their higher chemical stability. So, we must recognize that the chemical hardness is a useful concept for understanding the behavior of chemical systems. And it is coupled with the absolute electronegativity in this respect. From Fig. 3, one can found that the electronegativity of $Fe_{13-n}P_n$ ($n = 0$–13) clusters also displayed a clear downward trend besides a valley can be observed at Fe_1P_{12}. Because the larger the magnitude of χ_{M}, the stronger the ability to attract electrons to itself. So, the ability to attract electrons became weakened gradually with increases of valence electron count from P_{13} to Fe_{13}. In addition, the χ_{M} of Fe_1P_{12} is in a relatively obvious valley, which just means that the higher chemical inertness and the lower chemical activity. In fact, no matter the chemical hardness, chemical potential,

or electronegativity, they can only describe the chemical properties of a certain aspect of a metal cluster, which are difficult to describe the whole chemical properties of the metal cluster. Therefore, we expect to find and propose a more ideal parameter to describe the chemical stability of the metal cluster. Based on this, by analyzing the physical significance of chemical hardness and electronegativity,[24,25] we found that the chemical hardness of each cluster is used to be divided by its electronegativity, which can reflect the chemical properties of the target cluster in depth, and can increase the coupling between the ability of a resistance to change in the electron distribution in clusters and the ability to attract electrons, and we call it jyq $= \eta/\chi$ parameter. Namely, the higher the value of jyq $= \eta/\chi$ parameter, the higher the value of chemical hardness and the lower the electronegativity. In other words, the higher the value of jyq $= \eta/\chi$ parameter, the ability of the system to prevent electron redistribution is relatively stronger, and its ability to absorb electrons from the outside is relatively weakness. Whereas, if the lower the value of jyq $= \eta/\chi$, the stronger the ability to attract electrons from other system. In Fig. 3, one trough (Fe_2P_{11}) and two peaks (Fe_1P_{12} and Fe_7P_6) that can be found in the electron count dependence of the jyq parameter of the lowest-energy neutral $Fe_{13-n}P_n$ ($n = 0$–13) clusters. Which two peaks means the whole chemical stability of Fe_1P_{12} and Fe_7P_6 is higher than that of their neighboring chemical components. And one trough indicated that the chemical stability of Fe_2P_{11} is poor and its chemical activity is relatively higher, which could be attributed to its C_{2v} layered geometric structure with pentagonal bipyramid as intermediate layer. In addition, from Fe_2P_{11} to Fe_{13}, the chemical stability of binary Fe–P clusters gradually increases with the increase of the number of valence electrons that due to the ground state geometric structure of Fe–P clusters is gradually evolving from chain structure to cage (core-shell) structure in Fig. 1.

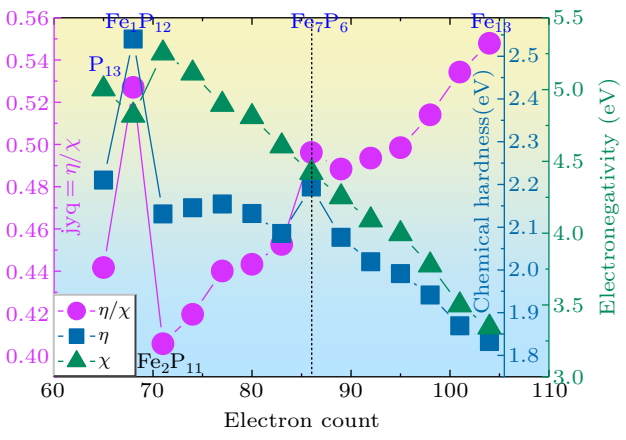


Fig. 3. The electron count dependence of the chemical hardness (η), electronegativity (χ), and jyq parameter of the lowest-energy neutral $Fe_{13-n}P_n$ ($n = 0$–13) clusters, respectively.

3.3. Electronic structure of the lowest-energy geometric structure of $Fe_{13-n}P_n$ ($n = 0$–13) clusters

The molecular orbitals of the lowest-energy neutral $Fe_{13-n}P_n$ ($n = 0$–13) clusters were plotted in Fig. 4, in order to analyze the electronic structure. From Fig. 4, one can found that the energy gaps of Fe_{13}, $Fe_{12}P_1$, $Fe_{11}P_2$, $Fe_{10}P_3$, Fe_9P_4, Fe_8P_5, Fe_7P_6, Fe_6P_7, Fe_5P_8, Fe_4P_9, Fe_3P_{10}, Fe_2P_{11}, Fe_1P_{12}, and P_{13} are 0.117, 0.06, 0.10, 0.147, 0.321, 0.273, 0.217, 0.251, 0.417, 0.348, 0.485, 1.278, 1.518, and 1.633 eV, respectively. The energy gap values of $Fe_{13-n}P_n$ ($n = 0$–13) clusters decrease in the following order: $P_{13} > Fe_1P_{12} > Fe_2P_{11} > Fe_3P_{10} > Fe_5P_8 > Fe_4P_9 > Fe_9P_4 > Fe_8P_5 > Fe_6P_7 > Fe_7P_6 > Fe_{10}P_3 > Fe_{13} > Fe_{11}P_2 > Fe_{12}P_1$, which indicates the P_{13} has the highest energy gap and the $Fe_{12}P_1$ has the lowest energy gap in the 14 chemical compositions in Fig. 4. Obviously, the P_{13} cluster shows typical insulator characteristics but the $Fe_{12}P_1$ shows typical conductor characteristics. Meanwhile, from the molecular orbital (MO) isosurfaces of $Fe_{12}P_1$, one can see that four π orbitals formed in the highest occupied molecular orbital (HOMO) with the components of 3d electrons of Fe, whereas several σ orbitals formed in the lowest unoccupied molecular orbital (LUMO) with the 3p and 3d electrons of Fe. For P_{13}, many stout σ orbitals formed in HOMO with the components of 2p electrons of the 13 P atoms with a chained geometric structure, similar σ orbitals formed in its LUMO with the components of the local massive pattern 2p electrons. So the obvious delocalized electrons in $Fe_{12}P_1$ cluster form a sharp contrast with the stronger localized electrons isosurfaces pattern in P_{13}, which provides a good physical explanation for the characteristics of conductors and insulators of $Fe_{12}P_1$ and P_{13} clusters, respectively. Next, in terms of nearly-free-electron mode,[26] the density of states (DOS) of the lowest-energy $Fe_{13-n}P_n$ ($n = 0$–13) clusters was calculated to investigate the correlation between the electronic structure and energy stability. For the lowest-energy $Fe_{13-n}P_n$ ($n = 0$–13) clusters, the curves of total DOS nearly the Femi level are plotted in Fig. 5. And the correlation between the electrons on the Femi level ($N(E_F)$) and the energy gap (E_g) dependence of the chemical components of the lowest-energy $Fe_{13-n}P_n$ ($n = 0$–13) clusters are plotted in Fig. 6. Combining Figs. 5 and 6, one can found that when Fe was replaced gradually with P from Fe_{13} to P_{13}, the $N(E_F)$ is obviously tended to toward a lower value, moreover, after $Fe_{10}P_3$, the $N(E_F)$ also shows odd–even oscillation effect in the decreasing trend. Whereas, the E_g shows an obviously increasing trend, especially when the difference between the number of P atoms and the number of Fe atoms become bigger and bigger. Namely, the maximum energy gap of P_{13} cluster corresponds to the Fermi level lies

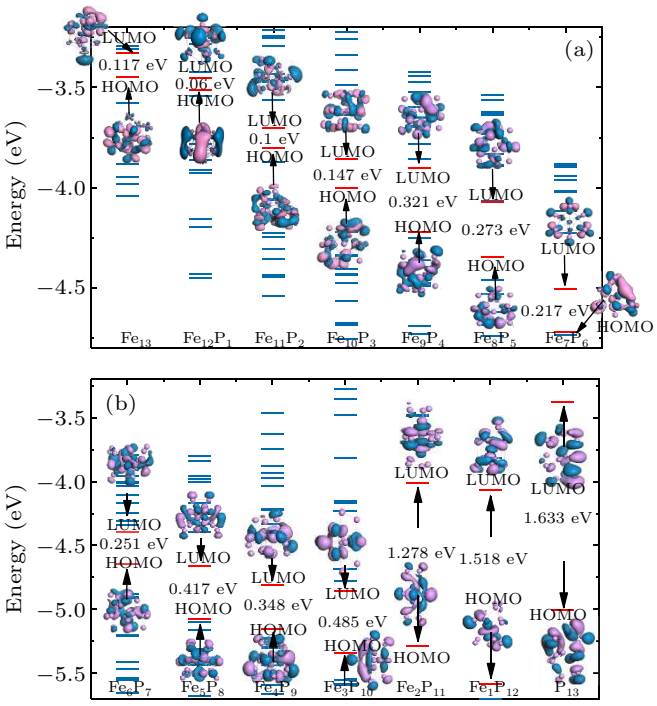


Fig. 4. Energy level and molecular orbital (MO) isosurfaces of the lowest-energy neutral $Fe_{13-n}P_n$ (n = 0–13) clusters. For interpretation of the references to color in this figure legend, the reader is referred to the web version of this article.

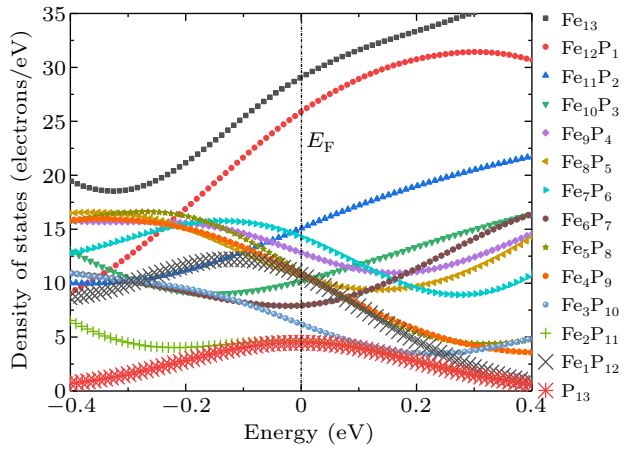


Fig. 5. Total density of states (DOS) near the Fermi level of the lowest-energy $Fe_{13-n}P_n$ (n = 0–13) clusters.

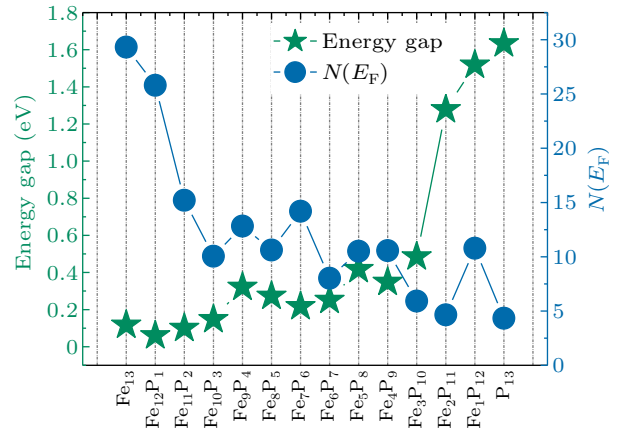


Fig. 6. Total $N(E_F)$ at Fermi level and energy gap dependence of the chemical components for the lowest-energy $Fe_{13-n}P_n$ (n = 0–13) clusters, respectively.

at a minimum of the density of states, and the minimum energy gap of $Fe_{12}P_1$ cluster almost have a maximum of the density of states on the Fermi level except of Fe_{13} cluster. Which means that the number of electrons on the Fermi level of Fe–P cluster mainly depends on its chemical composition, and which also further confirmed the objective fact that P_{13}, as an isolated free cluster with insulator characteristics could be attributed to having relatively few free electrons on the Fermi level.

3.4. Magnetic properties and atomic charge of the lowest-energy geometric structure of $Fe_{13-n}P_n$ (n = 0–13) clusters

To investigate the magnetic properties of the lowest-energy geometric structure of Fe–P clusters in Fig. 1, we have selected the density of states (DOS) curves of Fe_{13}, $Fe_{12}P_1$, Fe_7P_6, and P_{13} atomic clusters as the research objects in Fig. 7. In Fig. 7(a), perfect symmetrical spin-up and spin-down states can be observed for neutral Fe_{13} and P_{13} clusters, and remarkable asymmetries between spin-up and spin-down states can be observed for Fe_7P_6 and $Fe_{12}P_1$ clusters. These findings indicate that neutral $Fe_{12}P_1$ and Fe_7P_6 are ferromagnetic, whereas Fe_{13} and P_{13} clusters are not magnetic. In order to reveal the electronic orbits that have made substantial contributions to magnetism of Fe–P clusters, we had also plotted the curve diagram of the partial density of states of electrons, such as s, p, and d orbitals[27] in Fig. 7(b). From Fig. 7(b), one can find that asymmetrical total spin of Fe_7P_6 and $Fe_{12}P_1$ clusters could be attributed to the asymmetrical spin-up and spin-down states of d and p electrons, and s electrons also have a slightly split between spin-up and spin-down states and make a weakly contribution for the magnetic properties. Next, to investigate the correlation between the magnetic property[28] and Fe–P chemical composition, total magnetic dependences of the chemical components for the lowest-energy $Fe_{13-n}P_n$ (n = 0–13) clusters are plotted in Fig. 8. From Fig. 8, one can clearly find that the magnetic property is sharply decreased with the Fe replaced by P atoms one by one. Which indicates that Fe atoms still play a key role in generating magnetism for Fe–P clusters, even in the microscopic field they were dominated by quantum effects. Meanwhile, a non-magnetic property can be observed in Fe_{13}, Fe_2P_{11}, Fe_1P_{12}, and P_{13} that mainly because their perfect symmetrical between spin-up and spin-down states of electronic DOS.

Finally, in order to quantitative address the ionicity of A atom in the lowest-energy $Fe_{13-n}P_n$ (n = 0–13) clusters in Fig. 1, the Mulliken's charges $Q(A)$[29,30] of A atoms in the lowest-energy of $Fe_{13-n}P_n$ (n = 0, 1, 6, 13) clusters as typical representative is listed in Table 1. From Table 1, one can found that all the core atoms of Fe_{13} (I_h) and $Fe_{12}P_1$ (C_5) are posi-

tive, whereas all the shell atoms are negative. Namely, all shell atoms are to accept electrons in the formation of icosahedral cluster, different from the donation of core Fe. The charge transfer direction between Fe and P of $Fe_{13-n}P_n$ ($n = 0$, 1, 6, 13) clusters does not follow the Pauling's electronegativity, which revealed that the transfer of electrons in a free or isolated Fe–P cluster mainly depends on its geometric structure in some degrees. In fact, to compared with the Fe–P clusters in disordered atomic environment in MGs, the isolated ground state Fe_nP_{13-n} ($n = 3$–10) clusters usually have lower binding energy, fewer electrons on the Fermi level, stronger interatomic interaction, higher chemical stability, and lower chemical activity, and so on. Whereas, for Fe–P clusters in MGs, it is not only a metastable state, but also there are various interactions between the complex local atomic environment and the Fe–P clusters. So far, there is still a long way for the full understanding of the microscopic deformation mechanism of metallic glasses from the perspective of atomic cluster, three different approaches, experiments, computer simulations, and theoretical modeling, will be further closely combined well with each other in our future work.

Table 1. Mulliken's charges $Q(A)$ of A atoms in $Fe_{13-n}P_n$ ($n = 0$, 1, 6, 13) clusters.

	$Q(Fe_1)$ shell	$Q(Fe_2)$ shell	$Q(Fe_3)$ shell	$Q(Fe_4)$ shell	$Q(Fe_5)$ shell	$Q(Fe_6)$ shell	$Q(Fe_7)$ shell	$Q(Fe_8)$ shell	$Q(Fe_9)$ shell	$Q(Fe_{10})$ shell	$Q(Fe_{11})$ shell	$Q(Fe_{12})$ shell	$Q(Fe_{13})$ core
Fe_{13} (I_h)	−0.169	−0.152	−0.198	−0.191	−0.161	−0.181	−0.198	−0.191	−0.161	−0.152	−0.181	−0.169	2.104
	$Q(Fe_1)$ core	$Q(Fe_2)$ shell	$Q(Fe_3)$ shell	$Q(Fe_4)$ shell	$Q(Fe_5)$ shell	$Q(Fe_6)$ shell	$Q(Fe_7)$ shell	$Q(Fe_8)$ shell	$Q(Fe_9)$ shell	$Q(Fe_{10})$ shell	$Q(Fe_{11})$ shell	$Q(Fe_{12})$ shell	$Q(Fe_{13})$ shell
$Fe_{12}P_1$ (C_5)	1.923	−0.187	−0.198	−0.151	−0.156	−0.114	−0.160	−0.206	−0.197	−0.158	−0.205	−0.150	−0.041
	$Q(Fe_1)$	$Q(Fe_2)$	$Q(Fe_3)$	$Q(Fe_4)$	$Q(Fe_5)$	$Q(Fe_6)$	$Q(Fe_7)$	$Q(P_8)$	$Q(P_9)$	$Q(P_{10})$	$Q(P_{11})$	$Q(P_{12})$	$Q(P_{13})$
Fe_7P_6 (C_{3v})	0.043	0.426	−0.231	−0.215	0.031	0.048	−0.227	0.022	0.013	0.027	0.022	0.026	0.015
	$Q(P_1)$	$Q(P_2)$	$Q(P_3)$	$Q(P_4)$	$Q(P_5)$	$Q(P_6)$	$Q(P_7)$	$Q(P_8)$	$Q(P_9)$	$Q(P_{10})$	$Q(P_{11})$	$Q(P_{12})$	$Q(P_{13})$
P_{13} (C_1)	0.051	0.032	−0.001	−0.008	−0.094	0.004	0.021	−0.011	0.013	−0.007	0.031	−0.026	−0.006

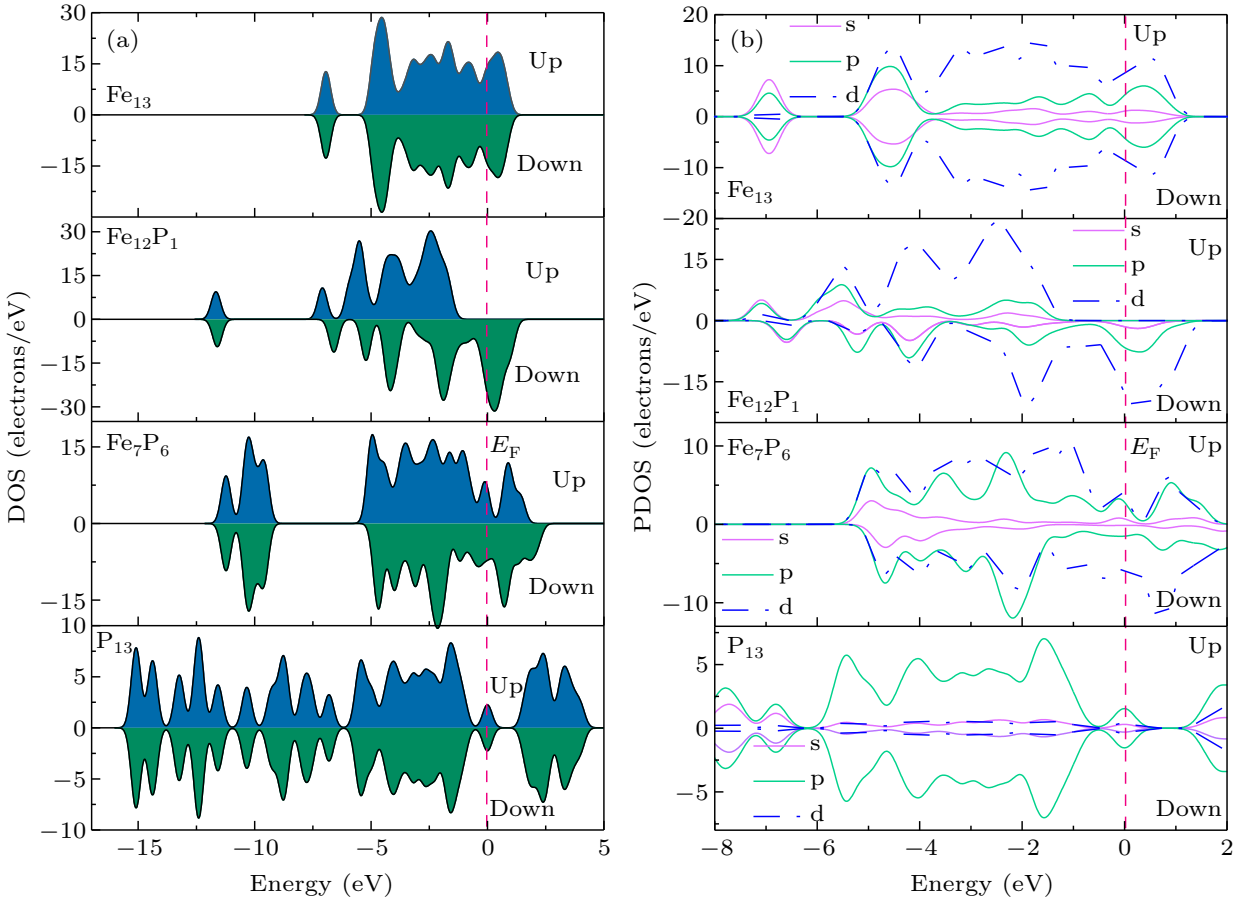


Fig. 7. (a) Total and (b) partial density of states (PDOS) regard as spin-up and spin-down states for the lowest-energy neutral $Fe_{13-n}P_n$ ($n = 0$, 1, 6, 13) clusters. The Fermi level indicated by the red dotted line is set to zero.

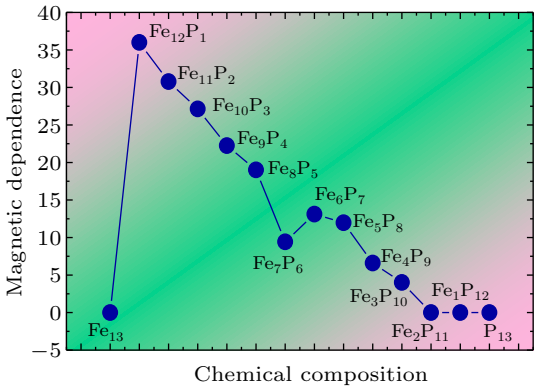


Fig. 8. Total magnetic dependence of the chemical components for the lowest-energy $Fe_{13-n}P_n$ ($n = 0$–13) clusters.

4. Conclusion

The ground state geometric structure of $Fe_{13-n}P_n$ ($n = 0$–13) clusters and their thermodynamical stability, chemical stability, electronic structure, and total magnetic dependence of the chemical components, were systematically investigated via DFT calculations in this paper. First, our research results show that the lowest-energy structure of the binary Fe–P clusters tend to form cage structures when the number of P atoms is less than the number of Fe atoms, but when the number of P atoms once exceeds Fe, the geometric structures of $Fe_{13-n}P_n$ ($n = 7$–13) clusters are gradually evolved to a chain shape from cage. And by analyzing the thermodynamical stability in terms of binding energy, our results show that the relationship between binding energy and chemical compositions of the lowest-energy $Fe_{13-n}P_n$ ($n = 0$–13) clusters is nonlinear. Second, by considering the physical significance of chemical hardness and chemical potential for Fe–P clusters, we have proposed a new parameter (jyq $= \eta/\chi$) that the chemical hardness is used to be divided by electronegativity to characterize the global chemical stability of the target cluster. The successful coupling ability of a resistance to redistribution of electrons and the ability to attract electrons from other atom, molecular or metallic clusters are one of the biggest advantages of jyq $= \eta/\chi$ parameter. Third, by analyzing the electronic structure (DOS, E_g, $N(E_F)$) of the lowest-energy geometric structure of $Fe_{13-n}P_n$ ($n = 0$–13) clusters, we found that the P_{13} cluster shows typical insulator characteristics but the $Fe_{12}P_1$ shows typical conductor characteristics, these phenomena can be attributed to obvious delocalized and localized electrons isosurfaces patterns in $Fe_{12}P_1$ and P_{13}, respectively. Moreover, the magnetic properties of the lowest-energy $Fe_{13-n}P_n$ ($n = 0$–13) clusters are sharply decreased with the Fe replaced by P atoms one by one, and a non-magnetic properties can be observed in Fe_{13}, Fe_2P_{11}, Fe_1P_{12}, and P_{13} that mainly caused by their perfect symmetries between spin-up and spin-down states of electronic DOS.

Acknowledgments

Project supported by the National Natural Science Foundation of China (Grant Nos. 52263025 and 51871096), the Scientific Research Project of the Education Department of Jiangxi Province, China (Grant Nos. GJJ2202021 and GJJ2202011), the Natural Science Foundation of Jiangxi Province, China (Grant Nos. 20202BAB204004 and 20171BAB216001), and the Qinglan Scholars Program and Scientific Research Project (Grant No. 22XJSK04) of Nanchang Normal University.

References

[1] Jena P and Sun Q 2018 *Chem. Rev.* **118** 5755
[2] Zhao J, Du Q, Zhou S and Kumar V 2020 *Chem. Rev.* **120** 9021
[3] Lee M S and Kanhere D G 2007 *Phys. Rev. B.* **75** 125427
[4] Sosso G C, Chen J, Cox S J, Fitzner M, Pedevilla P and Zen A 2016 *Chem. Rev.* **116** 7078
[5] He Y, Yi P and Falk M 2019 *Phys. Rev. Lett.* **122** 035501
[6] Cheng Y and Ma E 2011 *Prog. Mater. Sci.* **56** 379
[7] Lv J, Wang Y, Zhu L and Ma Y 2012 *J. Chem. Phys.* **137** 084104
[8] Wang Y, Lv J, Zhu L and Ma Y 2010 *Phys. Rev. B.* **82** 094116
[9] Wang Y, Lv J, Zhu L and Ma Y 2012 *Comput. Phys. Commun.* **183** 2063
[10] Zhang J, Liu H, Ma Y and Chen C 2022 *Natl. Sci. Rev.* **9** nwab168
[11] Sun Y, Liu H and Ma Y 2021 *Acta. Phys. Sin.* **70** 017407 (in Chinese)
[12] Sun Y, Lv J, Xie Y, Liu H and Ma Y 2019 *Phys. Rev. Lett.* **123** 097001
[13] Cui W W and Li Y W 2019 *Chin. Phys. B* **28** 107104
[14] Jiang Y Q and Peng P 2020 *Chin. Phys. B.* **29** 046105
[15] Jiang Y Q, Peng P, Wen D D, Han S C and Hou Z Y 2015 *Comp. Mater. Sci.* **99** 156
[16] Jiang Y, Lv J, He W and Peng P 2021 *J. Mol. Liq.* **343** 117603
[17] Shi J, Cui W, Hao J, Xu M, Wang X and Li Y 2020 *Nat. Commun.* **11** 3164
[18] Delley B 1990 *J. Chem. Phys.* **92** 508
[19] Delley B 2000 *J. Chem. Phys.* **113** 7756
[20] Ernzerhof M and Scuseria G E 1999 *J. Chem. Phys.* **110** 5029
[21] John P, Perdew K B and Ernzerhof M 1996 *Phys. Rev. Lett.* **77** 3865
[22] Bobadova-Parvanova P, Jackson K A, Srinivas S and Horoi M 2002 *Phys. Rev. B* **66** 195402
[23] Pearson R G 1986 *Proc. Nati. Acad. Sci.* **83** 8440
[24] Parr R G and Zhou Z 1993 *Acc. Chem. Res.* **26** 256
[25] Pearson R G 2005 *J. Chem. Sci.* **117** 369
[26] Nagel S R and Tauc J 1975 *Phys. Rev. Lett.* **35** 380
[27] Li Ji, Cheng X and Zhang H 2022 *Chin. Phys. B* **31** 097101
[28] Fu C, Huang J, Jiang Y and Li H 2022 *J. Phys. Chem. Lett.* **13** 6644
[29] Mulliken R S 1955 *J. Chem. Phys.* **23** 1841
[30] Segall M D, Shah R, Pickard C J and Payne M C 1996 *Phys. Rev. B* **54** 16317